

LETTER TO THE EDITOR

Recent star formation in the Lupus clouds as seen by *Herschel*[★]

K. L. J. Rygl¹, M. Benedettini¹, E. Schisano¹, D. Elia¹, S. Molinari¹, S. Pezzuto¹, Ph. André², J. P. Bernard³, G. J. White^{4,5}, D. Polychroni^{6,1}, S. Bontemps^{7,2}, N. L. J. Cox⁸, J. Di Francesco^{9,10}, A. Facchini¹, C. Fallscheer^{9,10}, A. M. di Giorgio¹, M. Hennemann², T. Hill², V. Könyves², V. Minier², F. Motte², Q. Nguyen-Luong¹¹, N. Peretto², M. Pestalozzi¹, S. Sadavoy^{9,10}, N. Schneider^{7,2}, L. Spinoglio¹, L. Testi^{12,13}, and D. Ward-Thompson¹⁴

(Affiliations can be found after the references)

Received ; Accepted

ABSTRACT

We present a study of the star formation histories of the Lupus I, III, and IV clouds using the *Herschel* 70–500 μm maps obtained by the *Herschel* Gould Belt Survey Key Project. By combining the new *Herschel* data with the existing *Spitzer* catalog we obtained an unprecedented census of prestellar sources and young stellar objects in the Lupus clouds, which allowed us to study the overall star formation rate (SFR) and efficiency (SFE). The high SFE of Lupus III, its decreasing SFR, and its large number of pre-main sequence stars with respect to proto- and prestellar sources, suggest that Lupus III is the most evolved cloud, and after having experienced a major star formation event in the past, is now approaching the end of its current star-forming cycle. Lupus I is currently undergoing a large star formation event, apparent by the increasing SFR, the large number of prestellar objects with respect to more evolved objects, and the high percentage of material at high extinction (e.g., above $A_V \approx 8$ mag). Also Lupus IV has an increasing SFR; however, the relative number of prestellar sources is much lower, suggesting that its star formation has not yet reached its peak.

Key words. Infrared: ISM – Stars: formation – Stars: protostars – ISM: individual objects: Lupus I, Lupus III, and Lupus IV

1. Introduction

In the current paradigm of low-mass star formation (SF), a gravitationally bound prestellar core will evolve into a young stellar object (YSO), passing through several phases, usually defined by Classes representing increasing stages of evolution: 0, I, II, and III (see André et al. 2000; Lada & Wilking 1984 for the definitions), before becoming a main-sequence star. While the later stages of low-mass SF are largely understood, less is known about the earlier stages (including the prestellar cores and the Class 0 objects) due to a lack of sensitivity and resolution at far-infrared to submm wavelengths. The *Herschel* Gould Belt Survey (HGBS, André et al. 2010), carried out with the *Herschel* Space Observatory (Pilbratt et al. 2010), aims at studying these early stages of SF in nearby molecular clouds forming the so-called Gould Belt (Comerón et al. 1992).

Located at a distance between 150 pc (Lup I and IV) and 200 pc (Lup III; Comerón 2008), the Lupus clouds (I, III, IV) are among the nearest star-forming regions in the Gould Belt. The large angular extent of the Lupus clouds across the sky ($334^\circ < l < 352^\circ$, $5^\circ < b < 25^\circ$) corresponds to a physical extent of 50 pc \times 55 pc at a distance of 150 pc, similar to the distance range among the Lupus I, III, and IV, clouds (50 pc). Previous *Spitzer* (Merín et al. 2008, hereafter M08) and molecular-line (Benedettini et al. 2012) studies of Lupus I, III, and IV have found that the three clouds seem to be at different stages of evolution: Lupus I is thought to be the youngest cloud, Lupus IV is a little more evolved, and Lupus III is the most evolved cloud.

The Lupus I, III, and IV clouds were mapped, as a part of the HGBS, at five wavelengths from 70 μm to 500 μm , covering the range where the spectral energy distribution (SED) of cold dust emission from prestellar sources and envelopes of Class 0/I objects (protostars), is likely to peak. Therefore, the *Herschel* data are crucial for detecting these objects and determining their physical parameters. The combination of the M08 catalog, containing mostly Class II/III pre-main sequence (PMS) stars, with the prestellar cores and Class 0/I sources detected by *Herschel* allows for a much more complete view of the ongoing SF in the Lupus clouds than previously possible. Here, we present the first-look letter of the SF history of the Lupus clouds. A detailed analysis of the *Herschel* data on Lupus and the resulting catalog of identified objects will be presented in a forthcoming first-generation paper (Benedettini et al. in prep.) and will be publicly available at the HGBS website¹.

2. *Herschel* observations and data reduction

The Lupus maps were obtained between January 2010 and January 2011 by photometric observations with the Photodetector Array Camera and Spectrometer (PACS; Poglitsch et al. 2010) and Spectral and Photometric Imaging Receiver (SPIRE; Griffin et al. 2010) in parallel mode using a scanning speed of 60'' s⁻¹. Map sizes are 2° \times 2° 3 for Lupus I and 1° 5 \times 1° 1 for Lupus III, covering a similar region as the *Spitzer* observations for both clouds. Lupus IV was imaged in two maps, 2° \times 1° 3 and 1° 3 \times 1° 3, covering the *Spitzer* map, as well as a new region, never mapped before at wavelengths of 160–500 μm . The data were exported from HIPE v 7.0 (Ott 2010) at level 0.5, and processed with the ROMAGAL data

[★] *Herschel* is an ESA space observatory with science instruments provided by European-led Principal Investigator consortia and with important participation from NASA.

¹ <http://gouldbelt-herschel.cea.fr/archives>

reduction pipeline (Traficante et al. 2011; Piazzo et al. 2012). The maps were astrometrically aligned with the $70\mu\text{m}$ MIPS images from the *Spitzer* ‘cores2disks’ (c2d) survey (Evans et al. 2003), which in turn have been aligned with 2MASS data, based on a number of point sources observed in both $70\mu\text{m}$ maps and yielding an astrometric precision of $\sim 2''$. Absolute flux calibration (see Bernard et al. 2010) was found to be better than 20% by comparing the *Herschel* data with the *Planck* and *IRAS* data in the same area. The resulting maps have beam sizes of $9''$, $12''$, $18''$, $25''$, $36''$, for $70\mu\text{m}$, $160\mu\text{m}$, $250\mu\text{m}$, $350\mu\text{m}$, and $500\mu\text{m}$, respectively. The Lupus I observations were affected by stray Moonlight, visible as a bright band in the declination direction of the map. Fortunately, this did not affect our compact source fluxes, since the background is removed in the procedure.

For computing column density and temperature maps, the 70 – $350\mu\text{m}$ maps were convolved to the $500\mu\text{m}$ resolution and rebinned to the same pixel size ($11''.5$). The pixel-by-pixel modified black-body fits were then performed on the regridded maps, excluding the $70\mu\text{m}$ map since this emission might not be tracing the cold dust exactly. For the modified black-body fitting we assumed a dust opacity of $\kappa_{1.3\text{mm}}=0.004\text{cm}^2\text{g}^{-1}$ (Hildebrand 1983), a grain emissivity parameter $\beta=2$, and the mean molecular weight $\mu=2.8$ (Kauffmann et al. 2008). The resulting column density map (Fig. A.1) was used to define the cloud area: the emission within the $A_V=2\text{mag}$ (assuming the column density to A_V relation of $N_{\text{H}_2}=9.4\times 10^{20}A_V\text{cm}^{-2}$, Bohlin et al. 1978) contour was considered cloud emission and the integrated column densities in this contour (Table 1) agree within 20% with the masses from the c2d extinction maps² (Chapman et al. 2009) within the same area.

Compact source detection and extraction were performed with CuTE_x (Molinari et al. 2011) in each of the five *Herschel* maps separately, using a 3σ SNR detection limit. Following Elia et al. (2010), sources across the five bands were associated according to their positions. We adopted a conservative approach and removed sources that had a displaced counterpart in the $350\mu\text{m}$ or $500\mu\text{m}$ bands by more than half of the FWHP from the source center common to the other bands, which can introduce a large uncertainty in the measured fluxes at the longer wavelengths. In particular, for the prestellar cores this could result in finding false objects by an overestimation of the mass (see next section). Sources with detection in fewer than three bands longward of $\lambda=70\mu\text{m}$ were discarded. We then fit a single temperature modified black-body function to the SEDs of the extracted sources, again excluding the $70\mu\text{m}$ flux, to derive dust temperatures. Source masses were then derived from the optically thin part of the modified black-body spectrum, using the same dust properties as above. The reduced chi-squared was used to remove sources with badly fitted SEDs, which would yield uncertain masses and temperatures otherwise, and hence could have a faulty prestellar core classification. Objects identified as non-Lupus members based on their proper motions (López Martí et al. 2011), in total 16 objects, were removed. We cross-checked our sample with the SIMBAD and the c2d database to remove known extragalactic sources (in total 13 galaxies were found). Seven off-cloud unresolved objects without a $70\mu\text{m}$ counterpart were classified as candidate galaxies and removed. Finally, to understand whether some of the off-cloud candidate protostars might have been misclassified (see Fig. A.1 and Sect. 4), we estimated the galaxy count completeness. Using the number counts from Clements et al. (2010), we find that for Lupus I and III we start lacking galaxies with flux

levels of $\sim 350\text{mJy}$ at $250\mu\text{m}$, while for Lupus IV the limit is 700mJy .

3. Results

Table 1. Properties of the Lupus clouds

Cloud	Lupus I	Lupus III	Lupus IV
distance ^a (pc)	150	200	150
coverage (degree ²) ^b	4.6	1.6	4.3
cloud area $>A_V=2\text{mag}$ (pc ²)	16.4	7.7	7.1
cloud mass $>A_V=2\text{mag}$ (M_\odot)	830	570	500
cloud mass $>A_V=8\text{mag}$ (M_\odot)	145	65	60
$N_{\text{tot}} = N_{\text{YSO}} + N_{\text{prestellar}}$	52	113	37
N_{YSO} 0/I/II/III ^c	1/10/10/4	1/10/50/42	3/9/11/4
$N_{\text{prestellar}}$	27	10	10
N_{unbound}	68	8	63

Notes. ^(a) See Comerón (2008) ^(b) SPIRE and PACS overlapping area. ^(c) Number of objects per Class 0, I, II, and III are based on the *Herschel* data and on the M08 catalog.

Figure A.1 shows that the Lupus clouds are overall elongated in shape and fragmented into smaller clumps, in which most of the pre- and protostellar objects are located. A prestellar core is defined as a gravitationally bound dense core (size $< 0.05\text{pc}$) without an internal luminosity source that will supposedly form stars in the future (see e.g., Ward-Thompson et al. 1994; di Francesco et al. 2007). We used the ratio of the core mass to its critical Bonnor-Ebert mass $\frac{M}{M_{\text{BE}}}$, to distinguish between prestellar cores and unbound objects that may or may not form stars (cf. Könyves et al. 2010), where M is the core mass, $M_{\text{BE}}=2.4Rc_s^2/G$ the Bonnor-Ebert mass (Bonnor 1956), c_s the sound speed ($c_s=\sqrt{k_B T/\mu m_H}$), R the radius, and T the core temperature. For the core mass, we used the mass obtained from the modified black-body fitting and computed the M_{BE} using the fitted modified black-body temperature and the deconvolved radius at $250\mu\text{m}$. Cores with $\frac{M}{M_{\text{BE}}} > 1.0$ are gravitationally bound (Bonnor 1956) and were classified as prestellar, while cores with a lower ratio were considered unbound objects. An example of prestellar core SED is given in Fig. 1.

A protostar is defined as a core that is internally heated by an embedded YSO and is still accreting material from its envelope. The presence of a YSO is ascertained by a $70\mu\text{m}$ and/or $24\mu\text{m}$ source (Könyves et al. 2010). Among the protostellar objects, the submm to bolometric luminosity ratio (André et al. 2000), $L_{\text{s2b}} = L_{\text{submm}}^{\lambda \geq 350\mu\text{m}}/L_{\text{bol}}^{\lambda \geq 3.4\mu\text{m}}$, derived from the *Herschel*, M08, and WISE data (Wright et al. 2010), was used to identify the protostars as Class 0 or Class I objects. Protostars with $L_{\text{s2b}} \geq 3\%$ were classified as candidate Class 0, while protostars with a lower ratio were identified as candidate Class I (a more conservative Class 0 definition than used by Bontemps et al. 2010). Examples of a Class 0 and a Class I SED are shown in Fig. 1. The classification of more evolved objects, i.e., the PMS stars (or Class II/III objects), was taken from M08 and SIMBAD. M08 also identified flat SED objects that trace the transition between Class I and II (Greene et al. 1994). Since we cannot distinguish between Class I and F sources with the *Herschel* data, we considered them as Class I objects.

With the conservative source selection (Sect. 2) and the classification described above, we found 47 candidate prestellar

² http://data.spitzer.caltech.edu/popular/c2d/20071101_enhanced_v1/

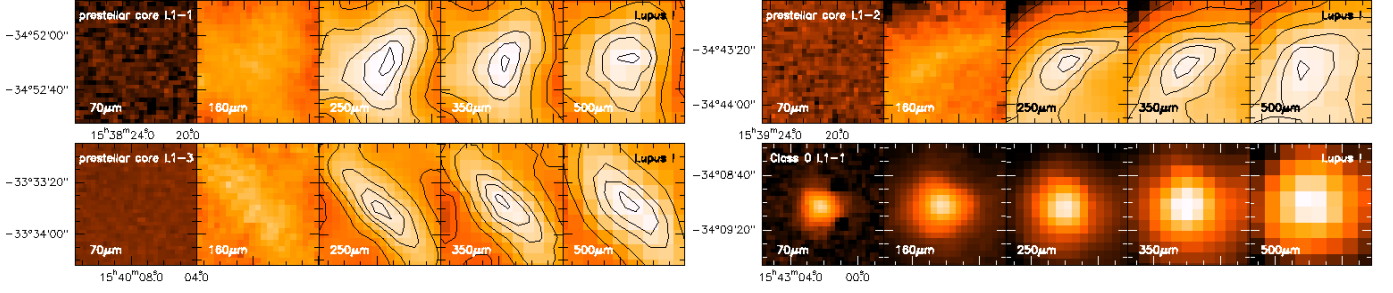


Fig. 2. Five-band images of three prestellar cores (contour levels are $\text{peakflux} \times 0.99, 0.95, 0.90, 0.80, 0.70, 0.60,$ and 0.50) and a Class 0 object in Lupus I. The maps are centered on the prestellar core/Class 0 object and are ordered by right ascension. The remaining prestellar and Class 0 sources of all three Lupus clouds are given in Fig. A.2.

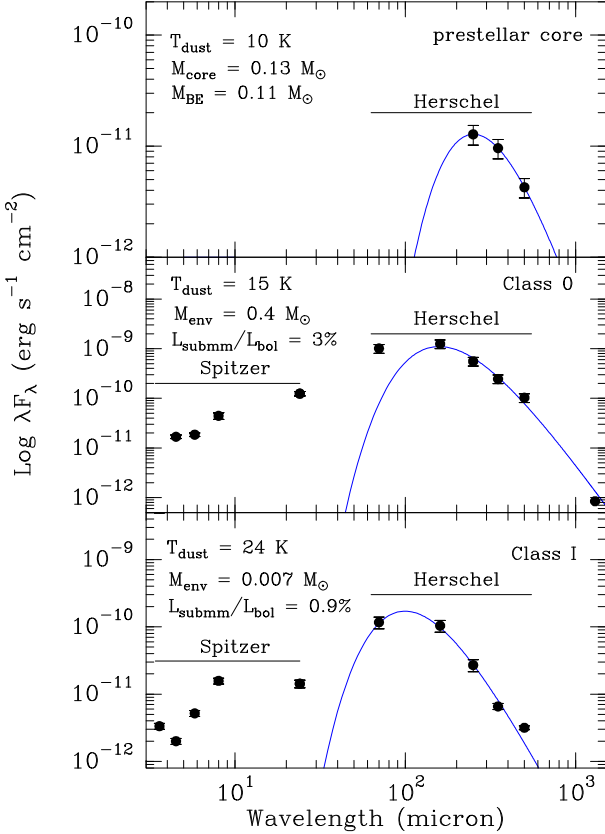


Fig. 1. Spectral energy distributions of a prestellar core, Class 0, and a Class I source in Lupus I and the modified black-body fit to the cold dust emission (blue line). The $3.4\text{--}24\ \mu\text{m}$ and $1300\ \mu\text{m}$ data points were taken from M08.

cores (see Fig. 2, continued in Fig. A.2, for all the five-band images). For the entire Lupus complex, the prestellar cores have median masses of $0.25 M_{\odot}$ within a range of $0.1\text{--}3.0 M_{\odot}$, and median temperatures of $9\ \text{K}$ within a range of $7\text{--}14\ \text{K}$. The mean prestellar source size is $0.02 \pm 0.01\ \text{pc}$. Five Class 0 sources were found (Figs. 2 and A.2), of which most were previously classified as Class I objects (M08). The only previously known Class 0 is Lup MM3 (Tachihara et al. 2007). The Class 0 temperatures are between $9.5\ \text{K}$ and $15\ \text{K}$. Their envelope masses ranged from 0.08 to $0.6 M_{\odot}$. For two Class 0 sources, we compared the dust temperatures obtained from the *Herschel* data to the kinetic temperatures obtained from ammonia (Benedettini et al. 2012), and found that they agree within 20%. We found 14 new Class I can-

didates in the Lupus clouds, 11 of which were outside the field covered by *Spitzer* c2d.

Table 1 summarizes the properties of the Lupus clouds and the objects found therein based on our results and the M08 catalog. The overlap between the *Herschel* data, including the YSOs that were only detected at $\lambda=70\ \mu\text{m}$ and $160\ \mu\text{m}$, with the M08 catalog was quite large, especially for the younger Class I objects. We detected 61% of their Class I objects, 46% of their Class II objects, and 10% of their Class III objects in the area covered by both surveys. For the few undetected Class I objects, we place an upper limit of $66\ \text{mJy}$ at $250\ \mu\text{m}$, and assuming a point source morphology, this implies a mass limit of $0.002 M_{\odot}$ at a dust temperature of $15\ \text{K}$.

4. Star formation history

Palla & Stahler (2000) posit that the star formation rate (SFR) has been increasing in the Lupus clouds over the past 4 Myr using number counts of PMS stars, whose ages they estimated through comparison with theoretical evolutionary PMS tracks. Our sample contains both prestellar cores and Class 0/I objects, and by merging with the M08 catalog we can, therefore, estimate the recent SFR behavior better than in previous studies.

One can deduce the relative number of objects N of a certain class with respect to a reference class expected for a constant SFR as $N=N_{\text{ref}} \times \tau / \tau_{\text{ref}}$ by assuming the classes' lifetimes τ and τ_{ref} . Since the Class II objects are expected to be complete (M08 and SIMBAD), we chose this as the reference class with the lifetime estimate of $2 \pm 1\ \text{Myr}$ (see Evans et al. 2009). For the other classes, we assume $0.5\ \text{Myr}$ for the prestellar lifetime (Enoch et al. 2008), $0.05\ \text{Myr}$ for the Class 0 lifetime (Froebrich et al. 2006), and $0.84\ \text{Myr}$ for the Class I lifetime (Evans et al. 2009). Using these lifetimes, we derived the expected numbers of objects in each Class (relative to the number of Class II objects). Figure 3 shows the ratio η of the observed-to-expected source numbers for the prestellar (η_{pres}), Class 0 (η_{Cl0}), and I (η_{ClI}) objects in each cloud. In this figure, we also plot the η_{ClI} without the possible galaxy contaminated sources (see Fig. A.1) based on the estimated completeness limit. Clearly, this possible contamination does not influence our SFR conclusions.

For both Lupus I and IV we find more prestellar, Class 0, and Class I objects than predicted for a constant SFR. We are therefore witnessing an increasing SFR over the past $0.5\text{--}1.5\ \text{Myr}$. The η 's, particularly the η_{pres} , is much larger in Lupus I than in Lupus IV, suggesting that Lupus I is undergoing a star formation event, while the SFR of Lupus IV might increase even more in the future. In Lupus III there are fewer prestellar, Class 0, and

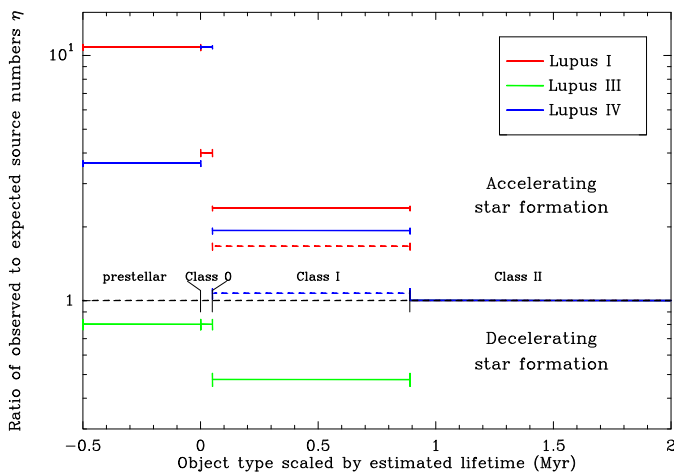


Fig. 3. Ratio of observed-to-expected (for a constant SFR) source numbers, η , per Class. Solid lines represent the numbers from Table 1, while dashed lines show Class I without the possible galaxy contamination.

Class I objects than expected for constant SFR. The star formation in Lupus III has decelerated over the past 2 Myr.

The SFR analysis depends heavily on the lifetimes used in the estimation. Performing the inverse analysis, assuming a constant SFR, and deriving the lifetimes (with respect to the number of Class II objects) would lead to lifetimes longer by a factor ~ 10 for the prestellar sources, ~ 4 for the Class 0 objects, and ~ 2 for the Class I objects in Lupus I. Finally, the results of this analysis do not depend on the source-finding algorithm, CuTex, since analysis of the sources found by *getsources* (Men'shchikov et al. 2012) yielded similar SFR trends.

We calculated the star formation efficiency (SFE), which is the ratio of the total mass in YSOs (Class 0 – III) M_s , assuming $0.2 M_\odot$ as the average Lupus PMS star mass (M08), to the total mass of the cloud plus YSOs: $\frac{M_s}{M_{cloud} + M_s}$. With this formulation, we find a similar SFE of $\sim 1\%$ in Lupus I and IV, but a much higher SFE of 3.5% in Lupus III. The latter may be expected from the high YSO-to-prestellar objects ratio (Table 1). The different distance of Lupus III, 200 pc, does not influence these results, because putting Lupus III at 150 pc magnifies its SFE to 6.1%.

One can study the star formation histories by interpreting the SFR behavior and SFE of the clouds as different evolutionary states within a star formation cycle. We propose that the high SFE of Lupus III, its decreasing SFR, and large number of PMS stars with respect to proto- and prestellar sources suggest that Lupus III is the most evolved cloud, which after having experienced a major star formation event, is now approaching the end of its current star-forming cycle. The properties of Lupus III seem to be similar to those of Chameleon I, where Belloche et al. (2011) claim to see the end of star formation based on prestellar cores found in $870 \mu\text{m}$ LABOCA data. On the other hand, Lupus I is currently undergoing a large star formation event, apparent by the increasing SFR and the large number of prestellar objects with respect to more evolved sources. Also Lupus IV has an increasing SFR; however, the relative number of prestellar sources is much lower, suggesting that its star formation has not yet reached its peak and that Lupus IV is at an earlier stage of evolution than Lupus I. The contrast between the increasing SFR in Lupus I and the decreasing SFR in Lupus III is possibly reminiscent of the contrast between L1688 and L1689 in Ophiuchus. There, L1688 is an active star-forming cloud with

many prestellar cores, while L1689 contains only a few prestellar cores, even though these clouds have similar CO properties. However, while Nutter et al. (2006) explain this difference by an external trigger from a nearby OB association, we claim that the diverse SFRs and SFEs in Lupus result from the clouds being in different states of their star formation cycle.

In Table 1 we also list the fraction of cloud mass above the SF threshold of $A_V \approx 8$ mag found in recent studies (e.g., Heiderman et al. 2010; André et al. 2010). This number, which is independent of source selection and identification, provides an estimate of the percentage of cloud mass directly available for SF, and it is expected to scale as the probability of finding prestellar cores. Spezzi et al. (2011) were the first to use this method on the extinction maps of the Lupus clouds. We applied this method to the *Herschel* data and found that Lupus I has a much higher percentage of mass above the A_V threshold than the Lupus III and IV clouds, supporting the idea of a star formation event in this cloud. Lupus IV has a only slightly higher percentage of dense material than Lupus III, as was also noted by Spezzi et al. (2011), supporting the similar number of prestellar cores found in these two clouds. The fraction of cloud mass above this A_V threshold correlates well with the number of prestellar cores found with *Herschel*, thereby strengthening our conclusions.

Acknowledgements. The authors thank the anonymous referee for her/his comments. SPIRE has been developed by a consortium of institutes led by Cardiff Univ. (UK) and including: Univ. Lethbridge (Canada); NAOC (China); CEA, LAM (France); IFSI, Univ. Padua (Italy); IAC (Spain); Stockholm Observatory (Sweden); Imperial College London, RAL, UCL-MSSL, UKATC, Univ. Sussex (UK); and Caltech, JPL, NHSC, Univ. Colorado (USA). This development has been supported by national funding agencies: CSA (Canada); NAOC (China); CEA, CNES, CNRS (France); ASI (Italy); MCINN (Spain); SNSB (Sweden); STFC, UKSA (UK); and NASA (USA). PACS has been developed by a consortium of institutes led by MPE (Germany) and including UVIE (Austria); KU Leuven, CSL, IMEC (Belgium); CEA, LAM (France); MPIA (Germany); INAF-IFSI/OAA/OAP/OAT, LENS, SISSA (Italy); IAC (Spain). This development has been supported by the funding agencies BMVIT (Austria), ESA-PRODEX (Belgium), CEA/CNES (France), DLR (Germany), ASI/INAF (Italy), and CICYT/MCYT (Spain). KLJR, ES, DE, MP, and DP are funded by an ASI fellowship under contract numbers I/005/11/0 and I/038/08/0. NLJC is supported by the Belgian Federal Science Policy Office via ESA's PRODEX Program.

References

- André, P., Men'shchikov, A., Bontemps, S., et al. 2010, *A&A*, 518, L102
 André, P., Ward-Thompson, D., & Barsony, M. 2000, *PPIV*, 59
 Belloche, A., Schuller, F., Parise, B., et al. 2011, *A&A*, 527, A145
 Benedettini, M., Pezzuto, S., Burton, M. G., et al. 2012, *MNRAS*, 419, 238
 Bernard, J.-P., Paradis, D., Marshall, D. J., et al. 2010, *A&A*, 518, L88
 Böhlín, R. C., Savage, B. D., & Drake, J. F. 1978, *ApJ*, 224, 132
 Bonnor, W. B. 1956, *MNRAS*, 116, 351
 Bontemps, S., André, P., Könyves, V., et al. 2010, *A&A*, 518, L85
 Chapman, N. L., Mundy, L. G., Lai, S.-P., & Evans, N. J. 2009, *ApJ*, 690, 496
 Clements, D. L., Rigby, E., Maddox, S., et al. 2010, *A&A*, 518, L8
 Comerón, F. 2008, *Handbook of Star Forming Regions II*, ed. Reipurth, B., 295
 Comerón, F., Torra, J., & Gomez, A. E. 1992, *Ap&SS*, 187, 187
 di Francesco, J., Evans, II, N. J., Caselli, P., et al. 2007, *PPV*, 17
 Elia, D., Schisano, E., Molinari, S., et al. 2010, *A&A*, 518, L97
 Enoch, M. L., Evans, II, N. J., Sargent, A. I., et al. 2008, *ApJ*, 684, 1240
 Evans, II, N. J., Allen, L. E., Blake, G. A., et al. 2003, *PASP*, 115, 965
 Evans, II, N. J., Dunham, M. M., Jørgensen, J. K., et al. 2009, *ApJS*, 181, 321
 Froebrich, D., Schmeja, S., Smith, M. D., et al. 2006, *MNRAS*, 368, 435
 Greene, T. P., Wilking, B. A., Andre, P., et al. 1994, *ApJ*, 434, 614
 Griffin, M. J., Abergel, A., Abreu, A., et al. 2010, *A&A*, 518, L3
 Heiderman, A. and Evans, II, N. J. and Allen, L. E., et al. 2010, *ApJ*, 723, 1019
 Hildebrand, R. H. 1983, *QJRAS*, 24, 267
 Kauffmann, J., Bertoldi, F., Bourke, T. L., et al. 2008, *A&A*, 487, 993
 Könyves, V., André, P., Men'shchikov, A., et al. 2010, *A&A*, 518, L106
 Lada, C. J. & Wilking, B. A. 1984, *ApJ*, 287, 610
 López Martí, B., Jiménez-Esteban, F., & Solano, E. 2011, *A&A*, 529, A108
 Men'shchikov, A., André, P., Didelon, P., et al. 2012, *A&A*, 542, A81

- Merín, B., Jørgensen, J., Spezzi, L., et al. 2008, *ApJS*, 177, 551, M08
Molinari, S., Schisano, E., Faustini, F., et al. 2011, *A&A*, 530, A133
Nutter, D., Ward-Thompson, D., & André, P. 2006, *MNRAS*, 368, 1833
Ott, S. 2010, in *ASP Conf. Series*, Vol. 434, 139
Palla, F. & Stahler, S. W. 2000, *ApJ*, 540, 255
Piazzo, L., Ikhenade, D., Natoli, P., et al. 2012, in *IEEE*, Vol. 21,
Pilbratt, G. L., Riedinger, J. R., Passvogel, T., et al. 2010, *A&A*, 518, L1
Poglitsch, A., Waelkens, C., Geis, N., et al. 2010, *A&A*, 518, L2
Spezzi, L., Vernazza, P., Merín, B., et al. 2011, *ApJ*, 730, 65
Tachihara, K., Rengel, M., Nakajima, Y., et al. 2007, *ApJ*, 659, 1382
Traficante, A., Calzoletti, L., Veneziani, M., et al. 2011, *MNRAS*, 416, 2932
Ward-Thompson, D., Scott, P. F., Hills, R. E., et al. 1994, *MNRAS*, 268, 276
Wright, E. L., Eisenhardt, P. R. M., Mainzer, A. K., et al. 2010, *AJ*, 140, 1868

Appendix A: Online Material

-
- ¹ Istituto di Astrofisica e Planetologia Spaziali (INAF-IAPS), via del Fosso del Cavaliere 100, 00133 Roma, Italy
e-mail: kazi.rygl@inaf.it
- ² Laboratoire AIM Paris-Saclay, CEA/IRFU CNRS/INSU Université Paris Diderot, 91191 Gif-sur-Yvette, France
- ³ CESR, Observatoire Midi-Pyrénées (CNRS-UPS), Université de Toulouse, BP 44346, 31028 Toulouse, France
- ⁴ Rutherford Appleton Laboratory, Chilton, Didcot, OX11 0NL, UK
- ⁵ Department of Physics and Astronomy, Open University, Milton Keynes, UK
- ⁶ University of Athens, Department of Astrophysics, Astronomy and Mechanics, Faculty of Physics, Panepistimiopolis, 15784 Zografos, Athens, Greece
- ⁷ CNRS/INSU, Laboratoire d'Astrophysique de Bordeaux UMR 5904, BP 89, 33271 Floirac, France
- ⁸ Instituut voor Sterrenkunde, KU Leuven, Celestijnenlaan 200D, 3001 Leuven, Belgium
- ⁹ Department of Physics and Astronomy, University of Victoria, PO Box 355, STN CSC, Victoria BC Canada, V8W 3P6
- ¹⁰ National Research Council Canada, Herzberg Institute of Astrophysics, 5071 West Saanich Road, Victoria BC Canada, V9E 2E7
- ¹¹ Canadian Institute for Theoretical Astrophysics (CITA), University of Toronto, 60 St. George Street, Toronto ON Canada, M5S 3H8
- ¹² European Southern Observatory, Karl-Schwarzschild-Strasse 2, 87548 Garching bei München, Germany
- ¹³ INAF-Osservatorio Astrofisico di Arcetri, Large E. Fermi 5, 50125 Firenze, Italy
- ¹⁴ Jeremiah Horrocks Institute, University of Central Lancashire, PR1 2HE, UK

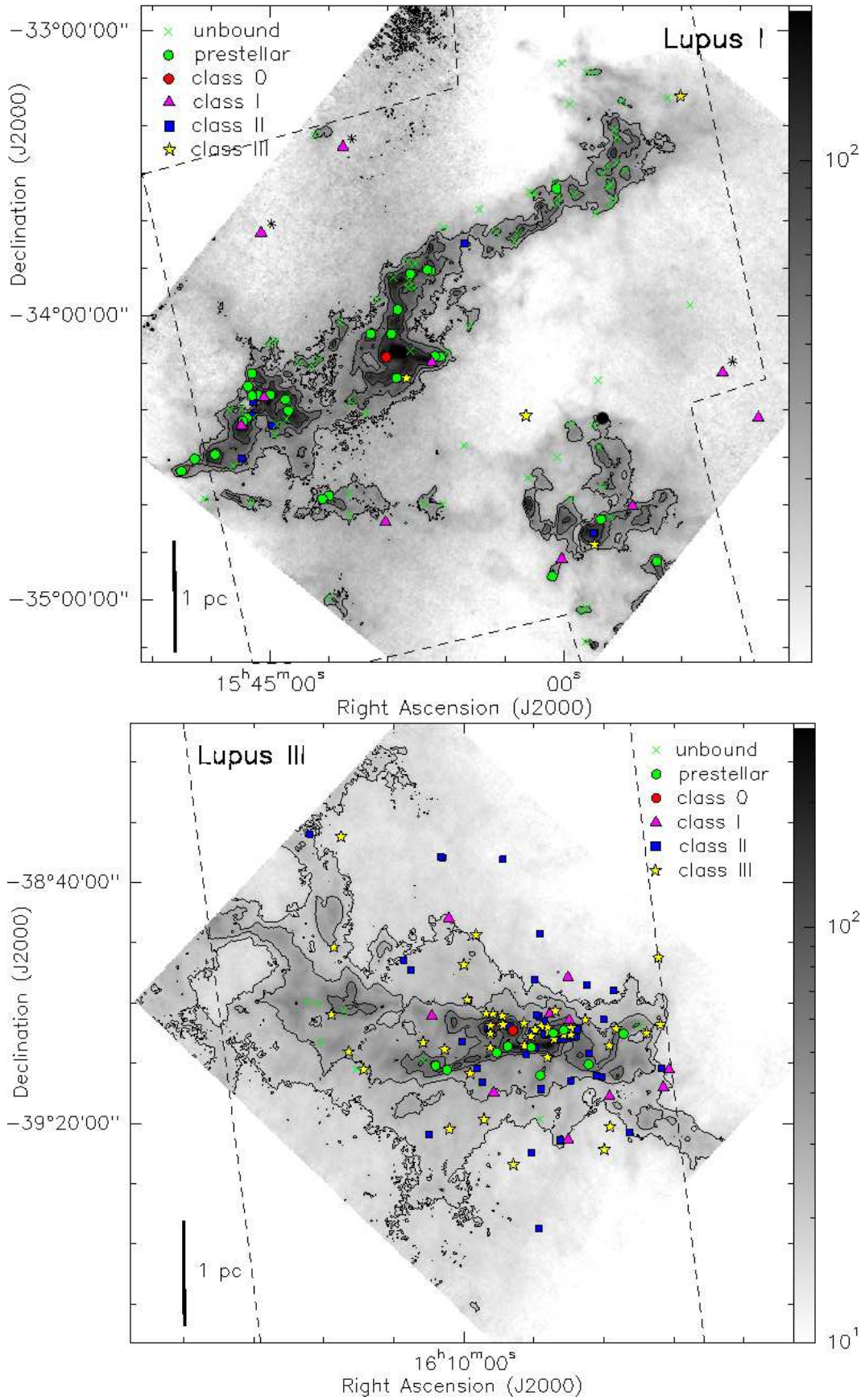


Fig. A.1. H_2 column density maps of Lupus I, III, and IV in units of 10^{20} cm^{-2} with A_V contours overplotted. For Lupus III and IV the contours are $A_V = 2, 3, 6,$ and 9 mag, while for Lupus I the contours are $4, 6,$ and 9 mag (to avoid the stray Moonlight). The different classes of objects, from the *Herschel* data and from the M08 catalog, are indicated. The off-cloud candidate Class I sources, marked by an asterisk, are those we considered as possible galaxy contaminations (shown by a dashed line in Fig. 3). The one off-cloud Class I in Lupus I without an asterisk has strong $24 \mu\text{m}$ emission, so is less likely to be a galaxy. Dashed contours mark the *Spitzer* MIPS coverage.

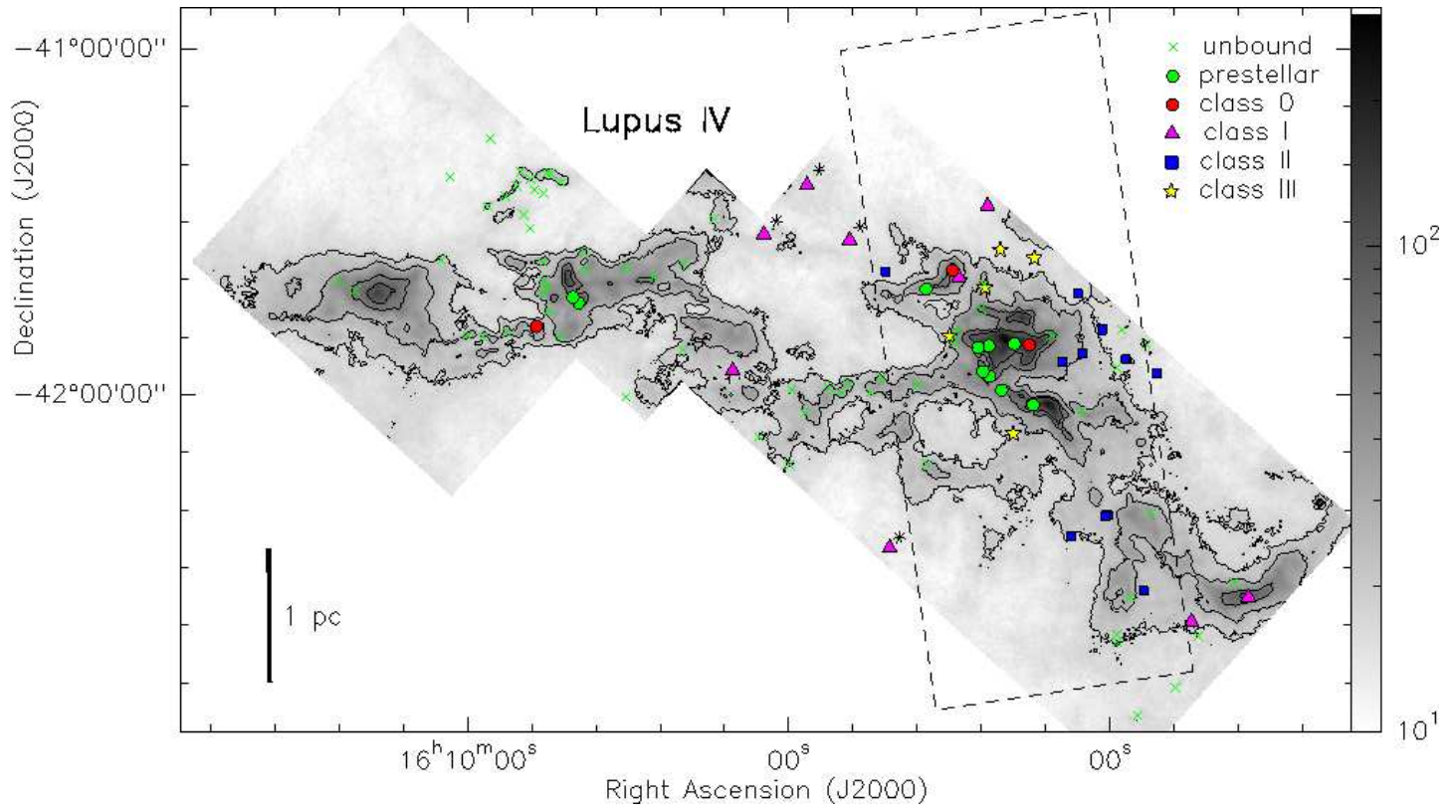


Fig. A.1. – *Continued*

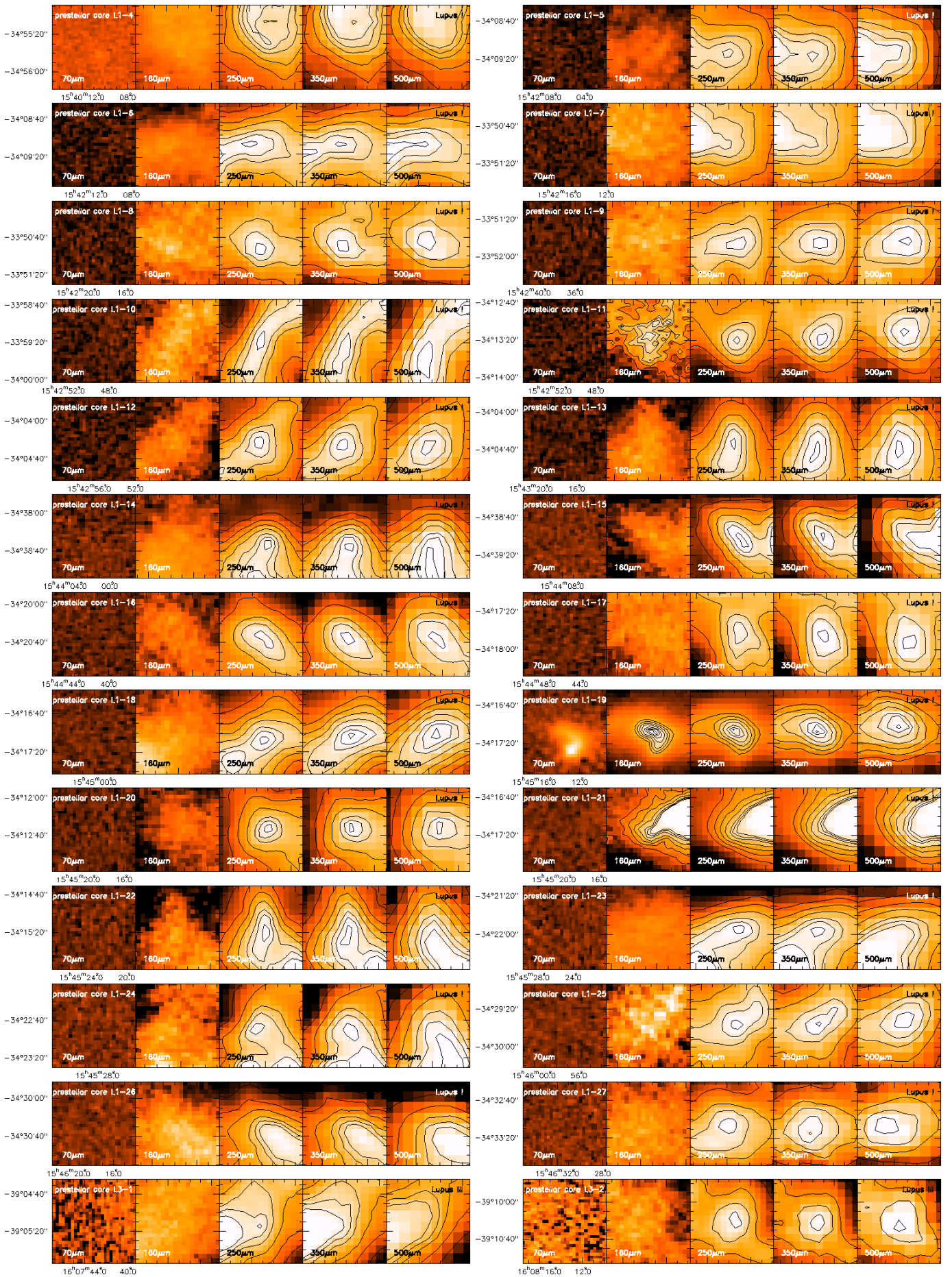


Fig. A.2. Visual catalog of the prestellar cores (contour levels are peakflux*0.99, 0.95, 0.90, 0.80, 0.70, 0.60, and 0.50) and Class 0 objects in the three Lupus clouds (I, III, IV), continued from Fig.2. The maps are centered on the prestellar core/Class 0 object and are ordered per cloud by right ascension.

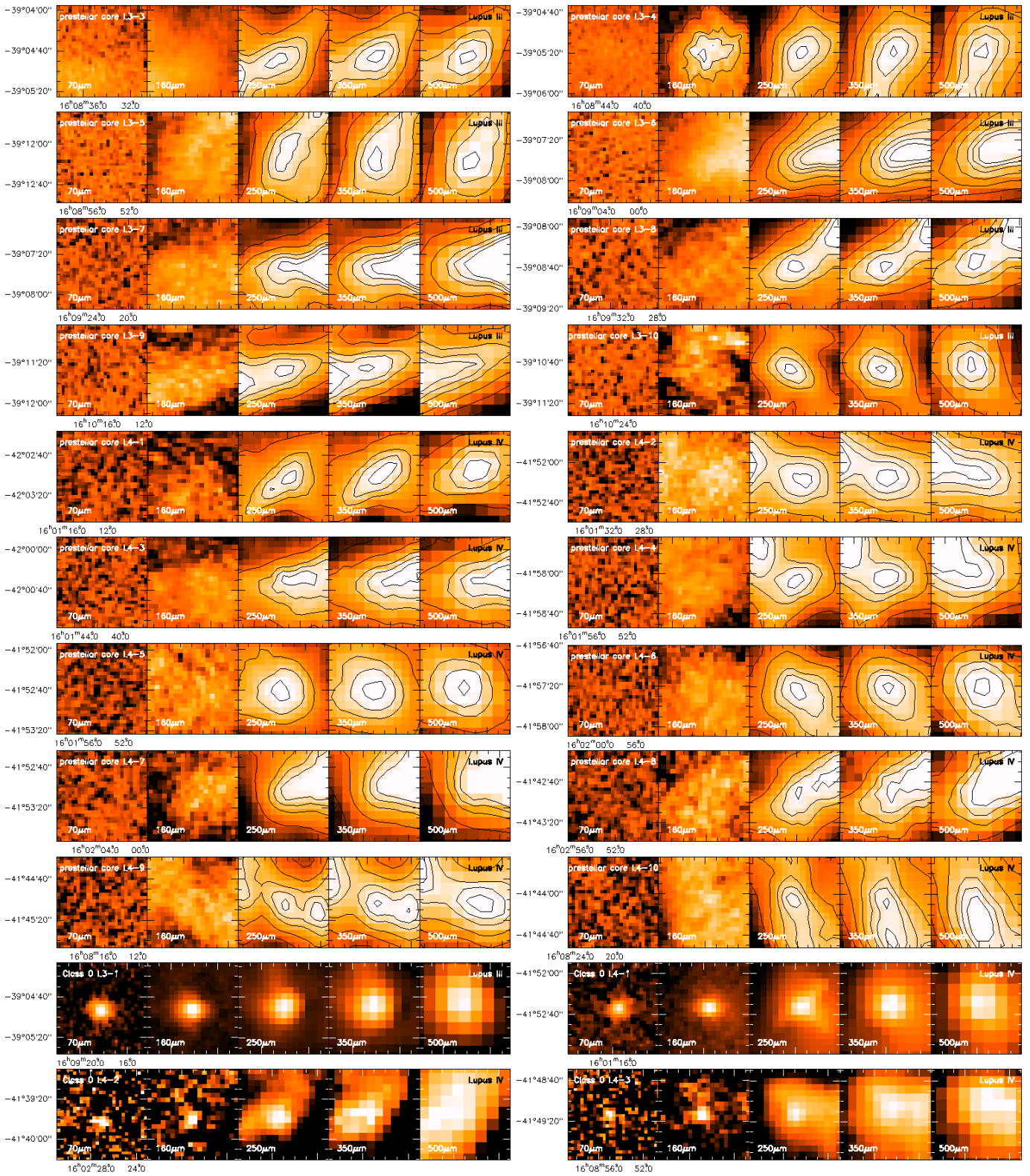


Fig. A.2. – *Continued*